The Effects of Pre-Oxidation of Cellulose on the Properties of Chars for Methane Storage

Fraser J. Norton, Gordon D. Love and Peter J. Hall
Department of Pure and Applied Chemistry
University of Strathclyde,
295 Cathedral Street Glasgow G1 1XL
SCOTLAND

Key words: Cellulose oxidation, methane storage, porosity formation.

Introduction

In the present economic climate and with ecological awareness at a high, the need for cheaper more environmentally friendly fuels has never been greater [1]. Natural gas is an abundant and relatively clean burning fuel. It is conventionally stored at high pressures for transportation and for use as an alternative vehicle fuel, (Compressed Natural Gas (CNG) pressure is 3000psi). Adsorbed Natural Gas (ANG) systems, which involve adsorption of gas onto porous media, (operating pressure, 500psi), have emerged as a viable alternative to CNG for use as a storage system for natural gas as a vehicle fuel. The methane is stored in the micropores (<20Å) of the adsorbent where the physical forces are such that the methane is at a higher density than that of liquid methane. Weaker forces in the meso (20-200Å) and macro-pores (>200Å) mean that compressed gas at 500psi only is stored in them. Since a finite volume (i.e. storage vessel) of adsorbent can be utilised, it is important that the adsorbent not only possesess high levels of microporosity, but that it is also of a high enough density. Activated Carbons contain high levels of microporosity and can be produced with satisfactorally high densities to be good adsorbents for methane storage. However, the process of creating an activated carbon generally involves gasification of the char with CO_2, O_2 or H_2O in order to increase the overall surface area. This treatment tends to widen the porosity and thus produce higher levels of meso- and macro-pores. By paying more attention to the precursor and the effects of altering its structure on the carbon produced, it may be possible to produce a more uniform microporosity. It was therefore decided to take pure cellulose and change its structure through air oxidation, observing any changes in the porosity of the resultant carbon produced.

Cellulose can be viewed as a linear condensation polymer consisting of D-anhydroglucopyranose units linked by β-1,4-glycosidic bonds [2]. The structure observed for the fully extended cellulose polymer is that of a flat ribbon with laterally protruding hydroxyl groups able to form both inter- and intra-molecular hydrogen bonds. Well-ordered areas of the cellulose structure contain hydrogen bonding between adjacent hydroxyl groups and the disordered areas show water bridging between adjacent chains [3]. The physical structure of cellulose has been studied using a variety of techniques including Differential Scanning Calorimetry (DSC). The difficulty in finding a first order phase transition in cellulose at a temperature lower than that of decomposition, (~500K) has been noted by Hatakeyama *et al* [4].

There has long been interest shown in the partial oxidation of cellulose by chemical means through the use of different reagents, mainly as a means of preventing damage to the cellulose structure during processes such as textile fibre and wood pulp bleaching [2]. However, utilisation of the product formed from physical oxidation through simple heating in an oxygen or air atmosphere of cellulose seems to have been somewhat neglected as a research field, probably because of its degrading effects on the cellulose

polymer. The oxidation of alkali cellulose by gaseous oxygen in order to reduce the degree of polymerisation of wood pulp for viscose rayon production has been the major application of this type of oxidation process, with a controlled degradation of the polymer being desirable.

Cellulose derivatives in the form of biomass are the most common source materials for the production of active carbons. A wide variety of cellulose derivatives varying from coal, lignite, peat, wood through to agricultural waste products are used commercially [5]. The range of activation conditions and methods is equally wide using lower temperature chemical activation [6], higher temperature steam or CO_2 activation [5], or a combination of both. The production of active carbons generally involves pyrolysis of cellulose bases in a highly oxidizing environment with the result that the pyrolysis is performed on oxidized cellulose.

The objective of the present paper is to investigate the effects of pre-oxidation of pure cellulose on the nature of chars produced by pyrolysis in N_2. This is achieved by characterization of the fresh and oxidized cellulose by a variety of common polymer analytical techniques, solid state NMR, (DSC) and elemental analysis. Mass losses during pyrolysis of the fresh and oxidized cellulose was monitored by thermogravimetric analysis (TGA). Characterization of the resulting chars was by nitrogen adsorption at 77K and BET analysis to yield surface area.

Experimental

Cellulose powder (20 micron) was obtained from the Aldrich Chemical company and used as supplied. Oxidation was performed at 473K for varying time in a forced circulation oven in air. Pyrolysis was performed in a tube furnace in a flowing nitrogen atmosphere. The carrier flow rate was 1 $lmin^{-1}$ and the sample size ~5g.

DSC was performed on a Mettler DSC 30 system. Temperature calibration was by the melting points of Indium, Lead and Zinc standards. Temperatures are accurate to ±0.5K. Enthalpy calibration was by integrating the melting endotherm of an Indium standard supplied by Mettler. It was estimated that enthalpies were accurate to ±0.05 J/g. Standard aluminium pans were used with two pin holes to allow evaporation of water and the removal of pyrolysis products. The sample size was 10mg. The polymer was spread in a monolayer over the base of the aluminium pans to maximize heat transfer to the cellulose. The procedure was as follows. The samples were dried *in situ* at 373K for 30 mins and then quenched to the starting temperature of 300K. DSC was then performed at 10K/min to a temperature of 523K using a nitrogen carrier. The samples were again quenched to 300K and DSC performed at 10K/min to 523K. The cycling procedure was repeated a further three times to identify only reversible phase changes in the samples.

25 MHz ^{13}C solid state nmr spectra of oxidised cellulose samples were obtained using a Bruker MSL100 spectrometer equipped with a 7-mm double-bearing probe for cross polarisation (CP) and magic angle spinning (MAS). The samples were spun at a speed of 5kHz, which is sufficient to reduce the side-band intensities to below 5% of those of the central aromatic bands in coals [7]. Typically four thousand scans were accumulated with high-power ^1H decoupling in CP experiments employing a contact time of 2ms and a recycle delay of 1.5s. Dipolar dephasing was carried out on one sample to estimate the fraction of non-protonated aromatic carbon present after oxidation. Delays of between 0-200μs were introduced immediately before acquisition during

which the ^1H decoupler was switched off. Those carbons bound to hydrogen are rapidly dephased while non-protonated and rotationally mobile (methyl) carbon dephase more slowly. The attenuation of the non-protonated aromatic carbon signal with increasing dephasing time follows a single exponential law. Thus by plotting ln(aromatic signal area) versus dephasing time and extrapolating the best line fit through data in the region 60-200μs to time zero, one can obtain an estimate of the fraction of non-protonated aromatic carbon. All FIDs were processed using exponential line broadening factors of 20Hz prior to Fourier transformation.

TGA was measured in a Stanton Redcroft TG750. A heating rate of 10 K/min was used and an air carrier. The typical sample size for TGA was ~10mg.

Surface area determinations were made from N_2 adsorption at 77K with a BET analysis. Samples were outgassed in situ to 10^{-4} Torr at a temperature of 398K for at least 12 hours before the adsorption was determined volumetrically in a Micromeretics Accusorb 2100E machine.

Results and Discussion

Chemical Composition Variation

Table 1 shows the ultimate analyses of the cellulose following the oxidation procedure described above. The O/C ratio decreases rapidly from 24 hours to 75 hours of oxidation and then shows a slight increase up to 456 hours. The initial decrease in oxygen content can be attributed to dehydration and, at the later stages of oxidation, loss of CO and CO2 on de-polymerisation of the cellulose. The slight increase in oxygen content from 75 hours to 456 hours is thought to be due to oxygen chemisorption by the cellulose. The H/C ratio decreases with an initial fast rate from 24 hours up to 75 hours of oxidation followed by a slower rate of H loss with time of oxidation and appears to be approaching some limiting value. Solid State ^{13}C NMR measurements were made to investigate the chemical changes on oxidation further. Figure 1 shows the NMR measurements on the oxidized cellulose samples. The aromatic/aliphatic ratios were determined by integrating the aromatic and aliphatic peaks which are indicated in Figure 1. The observed peaks were comparable to the accepted allocation of signals for cellulose [8]. The unoxidized cellulose showed no significant aromatic functionality, which is consistent with the accepted structure of cellulose [2]. However, even relatively mild oxidation was sufficient to produce a small aromatic content. This was corroborated by a colour change from white in the unoxidized cellulose to light brown in the 24 hour oxidized sample. The variation of the aromatic/aliphatic ratio with time of oxidation is shown in Figure 2. Initially, the ratio decreased slightly from a value of 0.152 for 24 hour oxidation to 0.106 following 50.5 hours of oxidation. The aromatic/aliphatic ratio then displayed a monotonic increase with time of oxidation up to 456 hours.

The decrease in H/C values may be associated with initial dehydration, (the O/C ratio decreased concurrently with H/C), accompanied by increasing aromaticity combined with the onset of cross-linking and more dehydration as the extent of oxidation increases. The variation of chemical composition based on C 100 together with the NMR data enables reasonable chemical structures to be constructed.

Figure 2 shows that the initial decrease in H/C ratio can not wholely be explained by simpley an increase in aromaticity. In fact the loss of hydrogen at this stage appears predominantly to be associated with an increase in crosslinkage of the cellulose

combined with dehydration.

The initial decrease in overall aromaticity of the oxidised samples up to 50.5 hours can be explained by the observed competitive generation of non-cellulose related aliphatics (at ~35ppm and 190ppm) in addition to the created aromatics (at~128,162ppm). An early indication of possible carbon crosslinking taking place is seen after 24 hours of oxidation (Figure 1a) when the C-6 signal (at ~70ppm) disappears. By 75 hours of oxidation, the cellulose structure has been completely altered (Figure 1b) and the cellulose peaks at have disappeared. The spectra at this stage consists of large aliphatic signals at 40ppm, due to alkyl groups, and 80ppm, due to ether groups, with a smaller aliphatic carbonyl signal at ~190ppm and aromatic peaks at 128ppm and 162ppm. The newly generated aromatic peaks at 128 and 162ppm dominate the NMR plots after 165 hours oxidation, with the new aliphatics at 40ppm and 80ppm taking a secondary role. The main aromatic peak centered at 128ppm corresponds to protonated and non-protonated aromatics (possibly bridgeheads for crosslinking), and the smaller peak at 162ppm corresponds to phenolic aromatics .

The general picture of changes on oxidation therefore appears to be an initial dehydration, occurring first at cellulose position C-6, with carbonyl production and generation of crosslinks with some aromatic production. This is followed by significant aromatic production with crosslinking by a mixture of short aliphatic groups and ether linkages.

Differential Scanning Calorimetry

The DSC plot, (Figure 3), for fresh cellulose shows a broad endotherm on run 1 from 330-400K due to the evaporation of water which was present on the surface of the polymer. After this water has been removed it can be seen that there is an endotherm indicative of a reversible second order phase transition probably due to a glass to rubber transition in the region 370-380K, which was obscured by the large evaporation endotherm. It has previously been observed by Hatakeyama *et al* [4] that dry cellulose exhibits no phase transition at a temperature below that of decomposition. This disagreement could arise from the fact that our own DSC sensor is somewhat more sensitive than that of Hatakeyama. Figure 4 shows the intensities of the glass transitions for the oxidised cellulose samples. The intensities of the Tg's are defined conventionally. It was noted that the Tg intensities decrease with increasing extent of oxidation. This may be due to an increase in cross-linking and density in the polymer which will make the structure considerably more rigid.

Oxidation and Carbonization

Table 2 shows the weight losses following oxidation and carbonization of the cellulose. The initial weight loss on oxidation up to 75 hours is extensive, with the loss from 75 hours to 456 hours being a lot smaller. The decomposition of cellulose in an oxygen atmosphere is well documented [9]. Initial weight loss is principally due to dehydration of water hydrogen bonded to the structure followed by dehydration of the actual cellulose structure, decarboxylation and general decomposition and depolymerisation of the cellulose. The weight loss after 75 hours being due mainly to hydrogen loss as the structure aromatises with some loss of CO and CO2. The carbon yields shown in Table 2 are the percentage of carbon in the original cellulose that remains in the char. The theoretical maximum carbon yield, if all of the carbon in the cellulose were converted into carbon in the char, is 68%. the char yield obtained for the untreated cellulose on carbonisation at 1173K using a heating rate of 10K/min of 18.4% is comparable to that quoted by Brunner and Roberts [10]. Increasing the extent of

oxidation decreases the overall carbon yield as more of the initial carbon in the cellulose structure is burnt away to form CO and CO_2 during the oxidation stage before carbonisation.

Thermogravimetric Analysis

Figure 5 shows the TGA plots for the oxidised cellulose samples. The samples show sleight weight loss from 300-500K. This is probably due to loss of adsorbed H_2O. An increase in the oxidation period promotes greater weight loss in this temperature range from 300-500K. This phenomena can be explained by the presence of polar oxygen groups on the polymer surface of the more highly oxidised samples and hence, on heating in the TGA, these samples will subsequently show greater weight losses over the 300-500K temperature range. The onset of pyrolysis can be observed for the samples after 500K. Rapid weight loss can be observed for the fresh and more mildly oxidised samples probably due to depolymerisation, and scission of C-O and C-C bonds within the cellulose ring units, accompanied with evolution of more H_2O, CO and CO_2 [3]. The more highly oxidised samples loose weight less rapidly than the less oxidised cellulose. This is because an increase in oxidation period causes an increase in weight loss during the oxidation process due to the loss mainly of H and O and some C and associated with this is an increase in cross-linking of the polymeric structure. Therefore the more highly oxidised samples contain less volatile species and are in fact much strengthened by cross-linking and so will lose less weight during pyrolysis. Mass transfer through the more heavily crosslinked structure will also be slower, thus allowing more time for carbonisation.

Surface Areas of The Carbons

Table 2 shows the 77K N_2 BET surface areas of the cellulose carbons. A clear trend can be seen whereby the surface area of the carbon increases with an increase in oxidation of the polymer precursor. The increase is an exponential rise which levels off at 456 hours oxidation, with a surface area nearly 9 times that of the fresh cellulose carbon. The similar physical properties of methane and nitrogen result in there being a close relationship between 77K N_2 BET surface area per unit mass of adsorbent and methane uptake. Large N_2 adsorption capacities are indicative of high levels of microporosity.

Conclusions

The cellulose structure goes through radical changes on air oxidation at 473K until, after 456 hours the structure bears little or no resemblance to the original polymer. Initial oxidation promotes dehydration of the cellulose, resulting in some aromatic formation and crosslinking of the structure. Further oxidation encourages extensive aromatic production combined with increased crosslinking, resulting in a highly aromatic, highly crosslinked network with increased strength and resistance to weight loss. The extent of oxidation is linked to the surface area of the carbon produced from the cellulose precursors. Increased oxidation period produced carbons with higher N_2 BET surface areas. The fresh cellulose probably produces large pores with a generally open structure on carbonisation, with the more highly oxidised cellulose developing a narrower porosity. Although these surface areas are a good representation of probable methane uptake, it is a high priority to carry out methane adsorption isotherms on the carbons. It is also intended to develop the porosity of the carbons through CO_2 activation followed by characterisation of the carbons with Hg porosimetry and Small Angle X-Ray Scattering. The pre-oxidation procedure has been shown to be a good method for controlling the porosity of unactivated cellulose precursor carbons.

References

[1] F.Stodolsky, d.Santini, "The Efficient Use Of Natural Gas in Transportation", Chem.Soc.Annual Meeting (1992)

[2] T.P. Nevell and S.H. Zeronian, Cellulose Chemistry and Applications, Ellis Horwood (1985)

[3] Cellulose: A review of the literature., Forestry Branch Departmental Publication No.1201, Ottawa (1967)

[4] T.Hatakeyama *et al*, Polymer, **23**, 1801 (1982)

[5] F.Rodriguez-Reinoso and M.Molina-Sabio, Carbon, **30**, 7, 1111 (1992)

[6] M.Jagtoyen and F.Derbyshhire, Carbon, **31**, 7, 1185 (1993)

[7] J.A.Franz, R.Garcia, J.C.Linehan, G.D.Love and C.E.Snape, Energy and Fuels, **6**, 598 (1992)

[8] M.Bardet *et al* ,Holzforschung, **40**, pp17-24 (1986)

[9] F.Shafizadeh, "Pyrolysis and Combustion of Cellulosic Materials"

[10] P.H. Brunner and P.V. Roberts, Carbon **18**,217(1990)

Table 1 Ultimate Analysis of Fresh and Oxidized cellulose

Sample	wt %C	wt %H	wt %O	H/C (g/g)	O/C (g/g)	arom/aliph
Fresh	42.41	6.46	51.13	0.152	1.21	
(C 100)	100	188	90			
24 hr	43.30	6.64	50.34	0.154	1.17	0.152
(C 100)	100	184	87			
44 hr	50.01	5.16	44.83	0.103	0.90	0.143
(C 100)	100	124	67			
50.5 hr	51.27	4.64	44.09	0.090	0.86	0.106
(C 100)	100	108	64			
75 hr	58.39	2.96	39.65	0.051	0.69	1.694
(C 100)	100	61	51			
165 hr	53.64	2.86	43.50	0.053	0.81	4.341
(C 100)	100	60	61			
456 hr	52.99	2.48	44.53	0.047	0.84	7.099
(C 100)	100	56	63			

Table 2 Pyrolysis Yields and Carbon Surface Areas

Sample	Wt loss on Oxidation (%)	Wt loss on Carbonization (%)	Carbon Yield (%)	BET SA (m^2g^{-1})
Fresh	-	81.6	18.4	65
150°C, 24 hr	4.0	80.7	19.1	414
150°C, 168 hr	9.4	80.0	18.2	384
200°C, 24 hr	9.9	80.2	17.8	360
200°C, 44 hr	38.3	69.9	18.6	415
200°C, 50.5 hr	44.3	67.9	17.9	420
200°C, 75 hr	65.4	57.4	14.7	459
200°C, 165 hr	76.2	59.5	9.6	507
200°C, 456hr	72.7	59.4	11.1	541

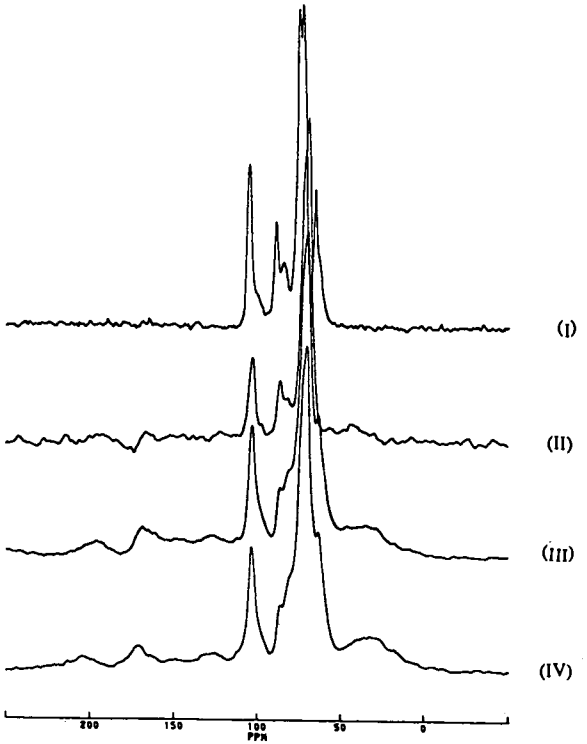

Figure 1(a) : ^{13}C NMR CP/MAS spectra of: Cellulose, (I) untreated, (II) oxidised at 473K for 24 hours, (III) oxidised at 473K for 44 hours, (IV) oxidised at 473K for 50.5 hours.

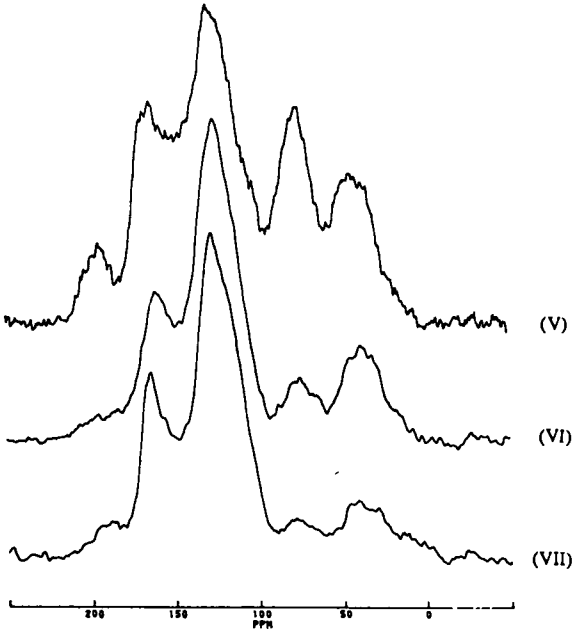

Figure 1(b) : ^{13}C NMR CP/MAS spectra of : Cellulose, (V) oxidised at 473Kfor 75 hours, (VI) oxidised at 473K for 165 hours, (VII) oxidised at 473K for 456 hours.

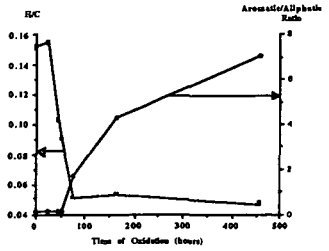

Figure 2 : Variation of H/C ratio and Aromatic/Aliphatic ratio with time of oxidation in air at 473K for cellulose powder. H/C values being derived from ultimate analysis and aromatic/aliphatic ratio from integration of the respective NMR peaks in Figure 1.

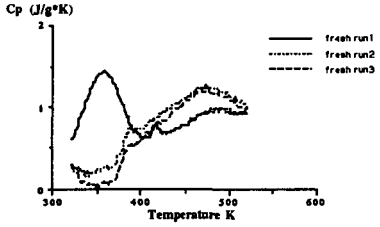

Figure 3 : DSC plot for untreated cellulose powder cycled from 323-523K in N_2 flow.

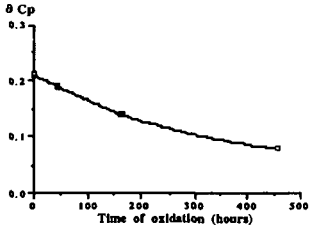

Figure 4 : Variation of δCp glass transitions of cellulose powder with time of oxidation in air at 473K.

MICROPOROUS CARBONS AS ADSORBENTS FOR METHANE STORAGE

D. F. Quinn, J. A. MacDonald and K. Sosin
Royal Military College of Canada, Kingston, Ontario

Keywords: Carbon Methane Storage

ABSTRACT

The volume available for gas storage is often limited. Because the density of the adsorbate is greater than the gas phase above it, gains in storage capacity at moderate pressures can be achieved through the use of adsorbents. Adsorbent storage systems can be used for various gases such as natural gas, hydrogen, ammonia or HFC's.

Optimal storage capacity will occur when that fraction of the storage volume that is micropore is maximized with no void or macropore volume. The average micropore diameter should be that most suited to the adsorbate molecule. In practice, this is difficult to achieve.

Carbons with high methane uptake per unit mass but with low bulk density may not be as suitable as carbons with lesser methane uptake but which have higher bulk density. The method of preparation of the adsorbent carbon is therefore very important. Conditions must be such that macropore formation is controlled and micropore enhanced.

INTRODUCTION

The acceptance of natural gas as a vehicular fuel has been slow, mainly due to a limited driving range. This range is restricted because of a much lower fuel or energy density than gasoline in the available storage volume. Initially an upper pressure of 2400 psi (16.3 MPa), equivalent to about 180 volumes of gas at STP per unit volume of storage, was used. This has been increased to 3000 psi (20 MPa), and even higher pressures have been called for.

The storage capacity of natural gas (methane) can be increased over that of compression alone through the use of an adsorbent. Methane density in a storage vessel at 3.4 MPa (500 psi) can be increased by a factor of four or more over that of compressed gas by using adsorbents, (1)(2). Thus through the use of carbons, methane storage densities of 180 V/V, equal to that of CNG at 2400 psi can be achieved at only one quarter or one fifth of the pressure, making adsorbed natural gas (ANG) an alternative to CNG. It should be noted here that storage is considered taking place at ambient temperature and cooling is not considered practical.

This increase in methane storage density in the storage vessel over CNG is due to adsorption of methane molecules in the micropore of the carbon. Therefore a carbon with a large micropore volume will adsorb more than one with a lesser micropore volume. However, these micropore volumes must be related to the storage vessel volume and not simply to a unit mass of carbon. The bulk or packing density of the carbon adsorbent therefore becomes very important.

When a vessel is packed with carbon, the volume occupied by the carbon atomic matrix is not available to methane. The fraction of the vessel volume which is void space or macropore volume will only store methane as compressed gas and that fraction which is micropore is the only one where there will be an increase in methane density. It follows, therefore, that a vessel packed without void space with a totally microporous carbon, maximized for microporosity, would be ideal.

Some carbons are closer to this ideal than others. The objective of this paper is to examine the characteristic properties of several carbons and relate these to methane storage. In doing this, it should be possible to consider different approaches to the preparation of adsorbent carbons in order to optimize them for methane storage.

Recent theoretical studies by Gubbins (3) and Myers (4) have shown that an optimal micropore would have a wall separation of about three to four methane diameters. The conclusion by Myers was that a highly idealized carbon composed of single graphitic layers 0.114 nm apart would store 209 V/V at 3.4 MPa.

Brookhaven National Laboratory have measured deliveries of methane from 3.4 MPa in excess of 150 V/V from carbon filled vessels at ambient temperature suggesting that storages of about 180 V/V have been achieved (5). Chaffee has prepared a carbon from Australian lignite which stored 202 V/V at 4.0 MPa (6).

EXPERIMENTAL

BET surface areas (7) and Dubinin-Radushkevich (8) micropore volumes for all the carbons were obtained using the Micromeretics ASAP 2000 to measure the nitrogen isotherm at 77K.

Mercury porosimetry measurements were carried out using the Quantachrome Autoscan 60 to obtain macropore volumes, and densities (9).

Methane isotherms were measured at 298K with the Sartorius M-25 high pressure balance. Buoyancy corrections were made by using equal weights of aluminum and magnesium as the counterweight. The deviation from ideality by methane was corrected using the data of Douslin et al. (10). For single stage compression, the practical benchmark pressure of 3.4 MPa (500 psi) was used in the comparison of the performance of each carbon.

TABLE 1

Carbons		BET Surface Area m^2/g	D-R Micropore Volume mL/g	Packing Density g/mL	Hg 1 atmos Particle Density g/mL	Mercury 60K psi Density g/mL	Macropore Volume mL/g	Methane Uptake 298K 500psia mgs/g
Norit	EX6	445	0.23	0.71	1.15	1.40	0.16	48
Calgon	SGL	900	0.4	0.49	0.78	1.33	0.53	65
Calgon	BPL	1030	0.47	0.44	0.75	1.11	0.43	75
Darco	Vapure 184-01	1095	0.51	0.58	0.81	1.19	0.39	84
ACCarbone	CNS 196	1190	0.49	0.44	0.85	1.22	0.36	80
Norit	R3	1270	0.58	0.42	0.65	1.06	0.80	92
Kureha	BAC	1350	0.60	0.59	0.90	1.08	0.19	99
California	GMS-70	1502	0.64	0.41	0.68	1.11	0.57	108
Barnebey	MI	1730	0.71	0.46	0.71	1.05	0.46	109
Sutcliffe	GS/60	1860	0.82	0.34	0.60	0.91	0.57	129
Osaka	M-30	2415	1.11	0.34	0.35	0.68	1.72	144
Kansai	Maxsorb	2671	1.29	0.27	0.29	0.90	2.34	164
Electrosynthesis	EL	2798	1.58	0.24	0.30	0.82	2.25	170

Table 1 lists the commercial carbons studied. These carbons come from a variety of precursors and have been made using different preparative methods. They cover a range of surface area and are listed on this basis. The Dubinin-Radushkevich micropore volume relates in a linear manner to the surface area. Methane uptakes at 3.4 MPa (500 psi) have been taken from the 298K isotherms, some of which are shown in Figure 1.

Figure 1

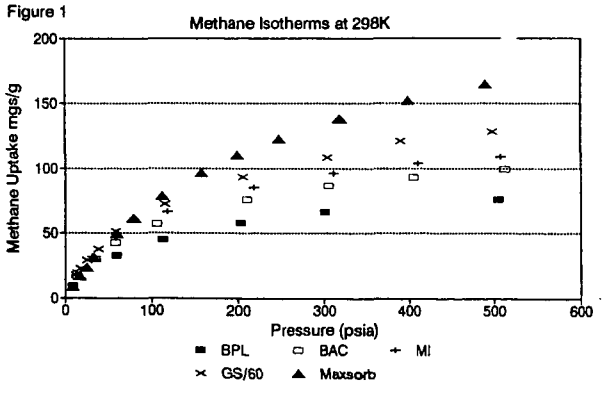

DISCUSSION

Many workers do not have the equipment to measure high pressure isotherms, but nearly every laboratory is able to measure surface areas and micropore volumes. Figure 2 shows the relationship between the 77K nitrogen surface area and the methane uptake at 3.4 MPa and 298K for these carbons. A more recent metbod, the alpba-s method, (11), distinguishes between micropore and surface area due to mesopore. This may be a better way of relating the extremely high surface area carbons to methane adsorption but has not been used in this paper. This relationship in Figure 2 is based on mass of adsorbent. The problem of gas storage is one of limited volume, and so the amount of methane which is stored in a vessel will be the product of the mass adsorption and the packed density of the carbon, plus methane stored as gas phase in the void and macropore volume.

Figure 2

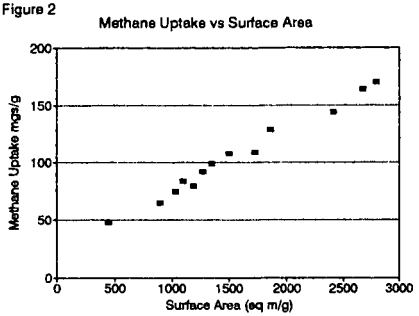

Figure 3

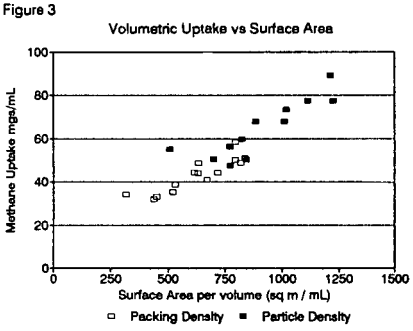

Because high surface area carbons often have low packing densities, they are often superseded in the amount of methane adsorbed per unit volume by carbons with greater packing densities. Figure 3 shows the surface area per mL with the methane adsorbed per mL of vessel using the normal packing density, (open squares). Additionally, Figure 3 illustrates the increase in adsorbed methane in the storage vessel if it could be packed to the particle density of the carbon. This latter situation is unrealistic but does serve to show the great gains to be made if packing density can be increased and voids reduced. The carbon which is most suited for methane storage is the Kureha BAC carbon, one of modest surface area per gram but which has both a high packing and particle density and low macropore volume. Figure 4 clearly shows that the high surface area per gram carbons are less suited for methane storage. Their large macropore volumes are mainly responsible for this.

Since storage of methane is taking place some hundred degrees above its critical temperature, adsorption will occur principally in the micropore. The methane density at 3.4 MPa and 298K in the micropore can be estimated. This has been plotted against the micropore volume per gram of carbon in Figure 5. Those carbons with large micropore volume (and high surface area) have low methane densities suggesting that the pore dimensions may be too large for efficient methane storage at temperatures well above its critical temperature.

Figure 4

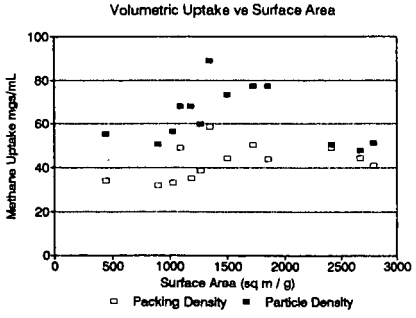

Dignum (12) has shown that the theoretical maximum density for methane at 298K is about 270 mgs/mL of pore. The low surface area Norit EX6 has a high methane density approaching this theoretical value. Takeda MSC-5A (13), a low surface area carbon, 445 m^2/g, has a methane

density in excess of 200 mgs/mL at 3.4 MPa and 298K. We have also found that unactivated coconut shell and peach pit chars of similar surface area to the Takeda carbon also have similar methane densities. This has also been shown for 5A and 13X molecular sieves (14).

Unfortunately all these materials have low micropore volumes per unit mass or volume and so are unattractive as candidates for methane storage. One carbon, made by the slow pyrolysis of PVDC polymer, has a methane micropore density of 219 mgs/mL at 3.4 MPa and 298K (15), suggesting that the pore dimensions are close to ideal. Additionally, about fifty percent of its particle volume is micropore with little or no macropore. It stores in excess of 150 V/V at 3.4 MPa and 298K.

Figure 5

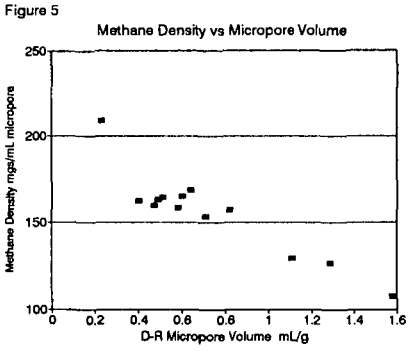

Traditionally carbons have been "activated" by heating them with air, steam or carbon dioxide at elevated temperatures. This results in carbons with higher surface areas per unit mass of carbon but with reduced packing and particle density. The reduction in density, however, is due not only to the creation of micropore but also to macropore formation. This macropore does not contribute to improved methane storage. The three high surface area carbons in Table 1 all have macropore volumes in excess of fifty percent of their particle volume.

The above shows that carbons can be made which have suitable micropore dimensions for methane storage, the problem is that these are not present in sufficient quantities to provide storage in excess of 180 V/V at 3.4 MPa and 298K. Methods of preparation which enhance micropore formation or reduce the production of macropore are desirable for gas storage carbons.

Figure 6

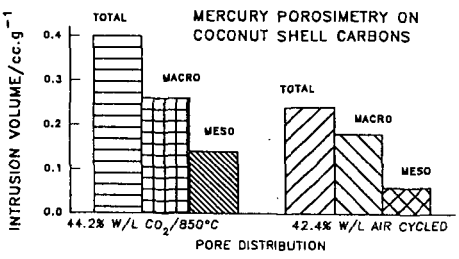

Figure 6 shows the meso and macropore volume for two CNS carbons. Both have been activated to about the same weight loss or burn off. One has been reacted with carbon dioxide at 850°C, a more conventional activation method. The other has been produced by cycling at low temperature with air followed by higher heat treatment under nitrogen (16). The latter method gave a carbon which had reduced macropore and mesopore volume, illustrated in Figure 6. It also had increased particle and packing density and showed an 18% increase in methane storage over the more conventionally prepared carbon.

Although storage has been emphasized in this paper, delivery from the storage vessel is perhaps more important. Delivery is considered as the amount of gas which is obtained from the vessel when the pressure is reduced to atmospheric. Carbons which have very narrow pore dimensions show high methane densities in these pores. They also have very steep Type 1 isotherms (17) and retain large amounts of methane at atmospheric pressure. PVDC carbon is a typical example of this type of carbon and retains at one atmosphere about thirty percent of the methane stored at 3.4 MPa. Treatment of this carbon with the air cycling technique improves the methane delivery.

Figure 7 relates carbon packing density and methane adsorption at 3.4 Mpa and 298K to delivery. The two curves for 100 and 150 V/V have been generated taking into account both the methane

desorbed isothermally and additionally the methane which would be stored as gas phase in void and macropore volume. The carbons from Table 1 are plotted using the normal packing density (open squares). They fall considerably short of the desirable 150 V/V delivered, however, if they were packed to their particle density (closed squares) then they come much closer to the goal.

Figure 7

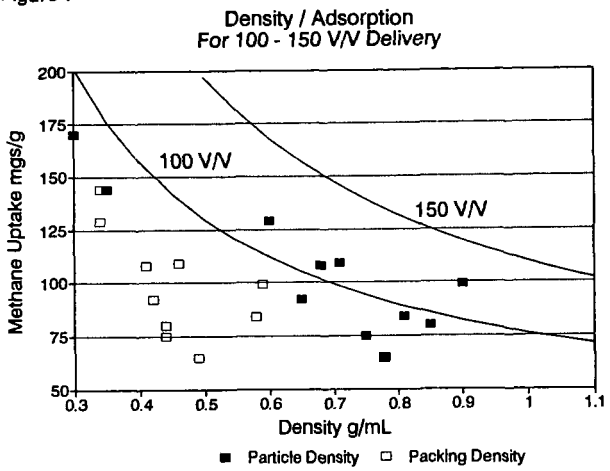

CONCLUSION

High surface area, low density carbons with high methane uptake per unit mass store and deliver less methane than some carbons with lower surface area but higher density. Carbons which have been optimized for micropore volume per unit volume will be most suited for ANG or other gas storage.

ACKNOWLEDGMENT

The authors wish to thank AGLARG, the Atlanta Gas Light Adsorbent Research Group, for their support for this study.

REFERENCES

1. J. Wegrzyn, H. Wisemann and T. Lee, SAE Proc. of Annual Automotive Technology Development, Nov 1992
2. C. Komodromos, S. Pearson & A. Grint, International Gas Research Confernce Proc. 1992, p588
3. Z. Tan and K.E. Gubbins, J Phys. Chem. 94 6061 (1994)
4. K.R. Matranga, A.L. Myers & E.D. Glandt, Chem. Eng. Sc. 47 1569 (1992)
5. J. Wegrzyn, Private communication, 1993
6. A.L. Chaffee, Proc. of Carbon 90, Paris, 1990
7. S. Brunauer, P.H. Emmett & E. Teller, J Amer. Chem. Soc. 60 309 (1938)
8. M.M Dubinin, E.D. Zaverina & L.V. Radushkevich, Zh. Fiz. Khim. 21 1351 (1947)
9. H.M. Rootare & C.F. Prenslow, J Phys. Chem. 71 2733 (1967)
10. D.R. Douslin, R.H. Harrison, R.T. Moore & J.P. McCullough,J Chem. Eng. Data 9 358 (1964)
11. P.J.M. Carrott & K.S.W. Sing in "Characterization of Porous Solids" p77 ed K.K. Unger et al, Elsevier (1988)
12. M.J. Dignum, Report 33259, Ontario Ministry of Transportation (1982)
13. S. Ozawa, S. Kusumi & Y. Ogino, J Coll. & Int. Sc. 56 83 (1976)
14. Y. Wakasugi, S. Ozawa & Y. Ogino, J Coll. & Int. Sc. 79 399 (1981)
15. D.F. Quinn & J.A. MacDonald, Carbon 30 1097 (1992)
16. U.S. Patent 5,071,820 (1991)
17. S. Brunauer, "Physical Adsorption of Gases and Vapours" Oxford University Press (1943)

MODELING THE FAST FILL PROCESS IN NATURAL GAS VEHICLE STORAGE CYLINDERS

Kenneth J. Kountz
Institute of Gas Technology
Chicago, IL 60632

Keywords: Natural Gas Vehicles, Gas Storage, Dynamic Gas Processes

INTRODUCTION

The on-board storage capacity of natural gas vehicles (NGVs) is a critical issue to the wide spread marketing of these alternate fueled vehicles. Underfilling of NGV cylinders, during fast fill (<5 min.) charging operations, can occur at fueling stations, at ambient temperatures greater than 50°F or 60°F. The resulting reduced driving range of the vehicle is a serious obstacle which the gas industry is striving to overcome, without resorting to unnecessarily high fueling station pressures, or by applying extensive overpressurization of the cylinder during the fueling operation. Undercharged storage cylinders are a result of the elevated temperature which occurs in the NGV storage cylinder, due to compression and other processes which have not, to the author's knowledge, been analyzed and documented to date.

This paper presents a model and solution methodology which quantifies the cylinder undercharging phenomena which occurs during rapid (<5 min.) fueling. The effects of heat transfer from the cylinder gas to its constraining walls and ambient are considered in the model analysis. The ramifications of the results on fueling station and cylinder designs are discussed. Suggestions are made for controlled experimental programs to verify the theoretical results, and for fueling station design studies which could minimize or eliminate cylinder underfilling.

ANALYSIS

MODEL ASSUMPTIONS

The following assumptions are made in the development of a mathematical model for fast charging natural gas cylinders.

1. The NGV cylinder is constant volume; there is negligible change in potential energy of the gas from the supply to the cylinder, and the kinetic energy of the cylinder gas is negligible. The pressure and temperature of the cylinder gas are not spatially dependent, i.e. quasi-steady perfect mixing occurs in the cylinder.
2. The mass flow, into the cylinder volume, is considered to be an isenthalpic expansion through an orifice.
3. The gas supply volume is infinite, with supply pressure and temperature remaining constant.
4. Heat transfer, from the cylinder control volume, is described by convective type heat flow to a lumped mass, cylinder wall. The cylinder wall temperature is not spatially dependent. Heat loss from the cylinder wall to the ambient is considered to be natural convection.

MODEL EQUATIONS

In applying the above assumptions to the natural gas storage cylinder charging model, shown in Fig. 1, one notes there are four basic dependent dynamic variables; the cylinder gas pressure, gas temperature, and mass of gas, and the lumped cylinder wall temperature. Four independent physical concepts are therefore needed for a dynamic solution.

The first physical concept applied is the dynamic energy equation for the NGV cylinder control volume, given in Equation (1). Note that each unit of supply gas, which enters the cylinder, has enthalpy, i.e. not only the internal energy of the gas in the supply, but also the supply "pv" work, associated with its flow. Note also that the gas in the cylinder volume contains only internal energy. One of the reasons behind the temperature rise of the gas in the cylinder, during a fast fill operation, lies in this conversion of enthalpy into internal energy.

The conservation of mass is the second physical concept utilized and is given in Equation (2). The supporting equations describing the assumed single orifice type flow rate are given in Equations (4) through (8). For adiabatic cylinder charging solutions of the set of modeled equations, the characteristics of the orifice, i.e. its area, rate of fill, or pressure ratio dependency will not affect the end temperature state in the cylinder, after a fill process to a given pressure. With heat transfer considered during cylinder charging, the flow rate characteristics of the orifice do influence the dynamic rates of heat exchange between the cylinder gas and cylinder wall, which in turn affects the end state cylinder gas temperature.

In this analysis, real natural gas properties are utilized to determine the property variables needed in the dynamic solution, i.e. enthalpy, internal energy, density, etc. These properties are obtained from subroutines which operate on pressure and temperature dependent tabulated results from the NIST computer program "STRAPP". The applicable equation of state, which provides a third physical concept, is given in Equation (3), or in its differential form, Equation (3a).

In deriving the basic differential equation set, reductions of Equations (1), (2), and (3) were used to solve for the NGV cylinder temperature, mass, and pressure respectively. The fourth dependent variable, the cylinder lumped mass wall temperature, is determined by the differential equation (10), after applying the supporting equations for the heat transfer into and out of the lumped mass wall, given in Equations (9) and (10) respectively. Fig. 2 shows a schematic of the cylinder wall heat transfer model.

SOLUTION PROCEDURE

The above described set of differential equations were numerically solved using the Runge-Kutta fourth order method, in a FORTRAN based computer program. Dynamic solutions for the cylinder gas pressure, temperature, and mass, and for the lumped cylinder wall temperature are output in the program together with integrated values for total heat transferred to and from the cylinder walls. Solutions end when the NGV cylinder pressure reaches a user-input pressure level.

MODEL RESULTS

TRANSIENT SOLUTIONS

Numerical solutions were developed using a mean U.S. natural gas composition whose components, by molar percentages are: Methane-92.87%, Ethane-3.34%, Nitrogen-2.07%, Carbon Dioxide-0.78%, Propane-0.63%, and less than 0.1% of I-Butane, N-Butane, I-Pentane, N-Pentane, and N-Hexane.

Examples of the dynamic pressure and temperature profiles in a 10" diameter, 50" long, NGV cylinder, during an adiabatic fill, are shown in Figures 3 and 4 respectively. In these results, the infinite supply gas conditions were 3000 psia and 70^{o}F, while the initial cylinder pressure utilized was varied between 100 psia, simulating a nearly empty NGV cylinder, to 2500 psia, which could describe the topping off of a vehicle storage tank. The orifice size for the charging process was chosen so that the cylinder would fill to within 10 psi of the 3000 psia supply level in about 4 minutes, when starting from a nearly empty, 100 psia cylinder. In actual fueling operations, from 50 to 100 psi minimum pressure difference may be necessary between the fueling station cascade supply and the cylinder, to accommodate the station metering requirements or other piping or filtration flow impedances.

Note, from Fig. 4, that the cylinder gas temperature dips significantly during the early stages of charging a nearly empty cylinder, before rising to a final level of about 145^{o}F. Note also that when charging a nearly full cylinder, the gas temperature profile is monotonic, reaching successively lower final values, as the initial pressure of the cylinder gas increases. The reason for the dip in temperature, in the early part of the filling of a nearly empty cylinder, lies in the

Joule-Thompson cooling effect, which the gas undergoes in the isenthalpic expansion through the orifice, from the 3000 psia supply pressure to the initially low 100 psia cylinder pressure. This cold gas mixes with and compresses the gas originally in the tank, with the result that the combined mixed gas temperature initially reduces. When the compression and conversion of supply enthalpy energy to cylinder internal energy overcomes the Joule-Thompson cooling effect, which becomes smaller as the cylinder pressure rises, the mixed gas temperature in the cylinder begins to rise. If the initial gas pressure in the cylinder is relatively high, the Joule-Thompson cooling effect is smaller, and does not, at any time, overcome the supply enthalpy conversion to cylinder internal energy. In this case, the cylinder gas temperature is seen to rise monotonically.

CYLINDER MASS FILL RATIOS

The charge parameter, which is directly related to the range of the NGV, is the cylinder "fill ratio", defined as the charged cylinder mass divided by the mass which the cylinder could hold at the rating condition of 70°F ambient and a pressure of 3000 psia. Fig. 5 shows how the mass fill ratio varies with initial cylinder pressure and supply pressure, for two values of the cylinder inside heat transfer coefficient. The adiabatic charge case corresponds to H_{cyl}=0 , while the H_{cyl}=5 Btu/(hr-sqft-F) results apply to a heat transfer coefficient which is 10 times the assumed ambient side natural convection transfer coefficient of H_{amb}=0.5 Btu/(hr-sqft-F).

The inside cylinder heat transfer coefficient is difficult to estimate, since the gas flow into the cylinder is highly dynamic, and depends on numerous fluid, orifice, and cylinder parameters which are themselves rapidly changing in the charging process. Experiments are suggested which might lead to the measurement of average values which could then be used for this coefficient.

As seen in Fig. 5, the consideration of the heat transfer to the cylinder wall, with the assumed H_{cyl}=5 Btu/(hr-sqft-F) value, provides little change in the mass fill ratio. With initial cylinder pressures up to about 1000 psia, the model results show that a NGV fast fill operation will only load the cylinder to about 80% of the rated mass level. Thus, unless H_{cyl} is found experimentally to average much larger than 5 Btu/(hr-sqft-F), little help can be expected from the heat transfer to the cylinder wall in alleviating the cylinder underfilling situation.

CYLINDER CHARGING REQUIREMENTS

NGV fueling stations must take into account at least ambient conditions when recharging cylinders to maximize the range of the vehicle, while at the same time avoid overcharging, with its possible safety problems.

Fig. 6 plots, for the adiabatic charge case, how the charged pressure in the NGV cylinder would vary with ambient temperature, to achieve a fully charged mass condition, defined as the rated mass in the cylinder at 3000 psia and 70°F. Note the influence of the supply pressure is small in determining the required charged cylinder pressure. The cooled pressure curve reflects the effect of ambient temperature on the rated cylinder mass.

As an example, if the ambient were 70°F, to achieve a cooled cylinder pressure of 3000 psia, the cylinder would need to be fast charged to about 4000 psia, if the supply gas were at 5000 psia. If the ambient were 100°F, the cylinder would need to be charged to about 4600 psia, to achieve the rated mass level.

This dynamic overpressurization is a source of design difficulty for not only the NGV cylinder manufacturer, but also for the fueling station manufacturer and operator, since the fueling station compressor discharge and ground storage would need to be at least 5000 psia, to insure a fully charged cylinder at high ambients.

NOMENCLATURE

Parameters and Variables		Units
A	= area	in^2
C_d	= orifice discharge Coefficient	--
C_p	= specific heat at constant pressure	$Btu/(lb_m\text{-}^oR)$
C_v	= specific heat at constant volume	$Btu/(lb_m\text{-}^oR)$
d	= differential	--
f	= functional	--
g_c	= dimensionalizing factor	$(lb_m\text{-}in)/(lb_f\text{-}sec^2)$
h	= specific enthalpy	Btu/lb_m
H	= convective heat transfer coefficient	$Btu/(in^2\text{-}sec\text{-}^oR)$
k	= ratio of specific heats, C_p/C_v	--
M	= mass	lb_m
P	= pressure	$(lb_f/in^2)_{abs}$
Q	= heat transfer	Btu
R	= gas constant	$(in\text{-}lb_f)/lb_m\text{-}^oR)$
t	= time	sec
T	= temperature	^oR
u	= specific internal energy	Btu/lb_m
V	= volume	in^3
W	= orifice flow rate	lb_m/sec
Z	= compressibility factor	--

Subscripts

amb = ambient

cyl = cylinder

r = receiver cylinder

s = gas supply

w = cylinder wall

1 = orifice

EFFECTS OF COOLING THE SUPPLY GAS

One opportunity, to alleviate the need for creating and storing such high pressures in the fueling station, lies in the cooling of the supply gas, if a practical and cost effective way could be developed.

Fig. 7 shows the effects of cooling the supply gas, assumed to be at 4000 psia, to various temperature levels. As in Fig. 6, these results were created from the model for the adiabatic charge scenario. Note that by cooling the supply gas to 60°F, the required charged pressure, even at 100°F ambient, is reduced to about 3950 psia, to achieve a fully charged cylinder status.

RECOMMENDATIONS FOR FUTURE RESEARCH

Future research is recommended in three areas associated with the fast fill NGV problem. First, additional model development is needed to consider finite supply reservoirs, in a commonly used cascade group of three, which might be designed and controlled during the fast fill operation to reduce the temperature rise in the NGV cylinder. Second, experiments are proposed to support the model development, on well instrumented cylinders. Dynamic measurement of the mass entering the cylinder is needed to assure a proper model of gas flow rate profile. Experiments with the supply reservoir ambient at lower temperatures, relative to a cylinder located in a lab environment, would simulate the theoretically large supply gas cooling effect. Lastly, research and design studies are recommended to determine practical ways of cooling and storing the gas supply in the fueling station.

LIST OF EQUATIONS

Energy Balance

$$\frac{dQ_r}{dt} + W_1 h_s = \frac{d}{dt}\left(M_r u_r\right) \tag{1}$$

Conservation of Mass

$$\frac{dM_r}{dt} = W_1 \tag{2}$$

Equation of State

$$P_r V_r = R Z_r M_r T_r \tag{3}$$

in differential equation form, with V_r = constant

$$v_r \frac{dP_r}{dt} = R \frac{d}{dt}\left(Z_r M_r T_r\right) \tag{3a}$$

Orifice Flow Equation

$$W_1 = C C_{d_1} A_1 \frac{P_s}{\sqrt{T_s}} f\left(\frac{P_r}{P_s}\right) \tag{4}$$

where

$$C = \sqrt{\frac{g_c k}{R\left(\frac{k+1}{2}\right)^{\left(\frac{k+1}{k-1}\right)}}} \tag{5}$$

$$f\left(\frac{P_r}{P_s}\right) = 1 \text{ for } \frac{P_r}{P_s} \leq \left(\frac{P_r}{P_s}\right)_{crit} \tag{6}$$

$$f\left(\frac{P_r}{P_s}\right) = \sqrt{\left(\frac{2}{k-1}\right)\left(\frac{k+1}{2}\right)^{\left(\frac{k+1}{k-1}\right)}}\left(\frac{P_r}{P_s}\right)^{\left(\frac{1}{k}\right)}\sqrt{1-\left(\frac{P_r}{P_s}\right)^{\left(\frac{k-1}{k}\right)}} \qquad (7)$$

$$\text{for } \frac{P_r}{P_s} > \left(\frac{P_r}{P_s}\right)_{crit}$$

$$\left(\frac{P_r}{P_s}\right)_{crit} = \left(\frac{2}{k+1}\right)^{\left(\frac{k}{k-1}\right)} \qquad (8)$$

Heat Flow Into Cylinder Wall

$$\frac{dQ_r}{dt} = -H_{cyl}A_{cyl}(T_r - T_w) \qquad (9)$$

Heat Flow From Cylinder Wall to Ambient

$$\frac{dQ_{amb}}{dt} = H_{amb}A_{cyl}(T_w - T_{amb}) \qquad (10)$$

Cylinder Wall Temperature

$$\frac{dT_w}{dt} = \frac{1}{M_w C_{p_w}}\left(\frac{dQ_w}{dt}\right) \qquad (11)$$

$$\frac{dT_w}{dt} = \frac{1}{M_w C_{p_w}}\left(-\frac{dQ_r}{dt} - \frac{dQ_{amb}}{dt}\right) \qquad (11a)$$

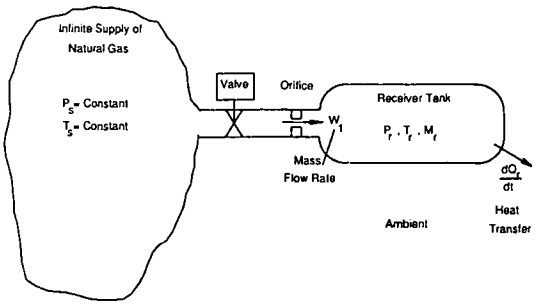

Fig. 1 Natural gas storage cylinder charging model

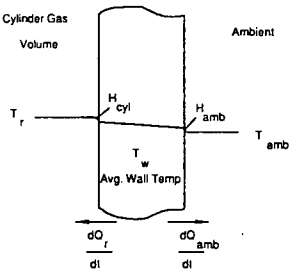

Fig. 2 Model of heat transfer through cylinder wall

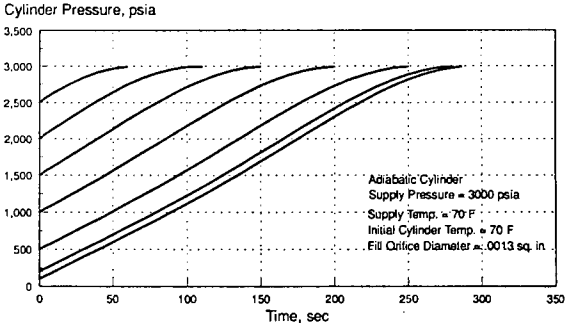

Fig. 3 Pressure in a 10"x50" Aluminum cylinder during a 3000 psia charge

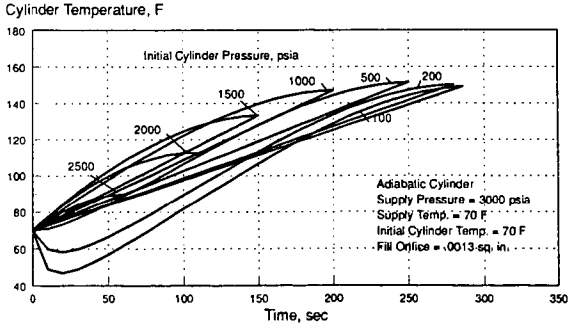

Fig. 4 Temperature in a 10"x50" Aluminum cylinder during a 3000 psia charge

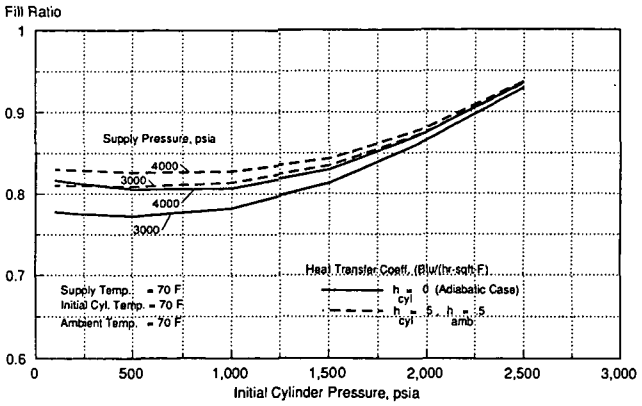

Fig. 5 Natural gas fill ratio in a 10"x50" Aluminum cylinder at the end of a 3000 psia charge

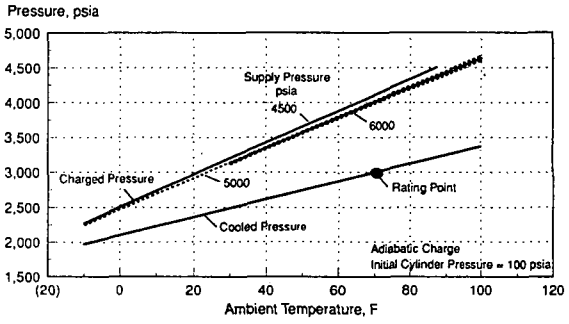

Fig. 6 Charged and cooled cylinder pressures for the rated charged mass, at 3000 psia and 70 F

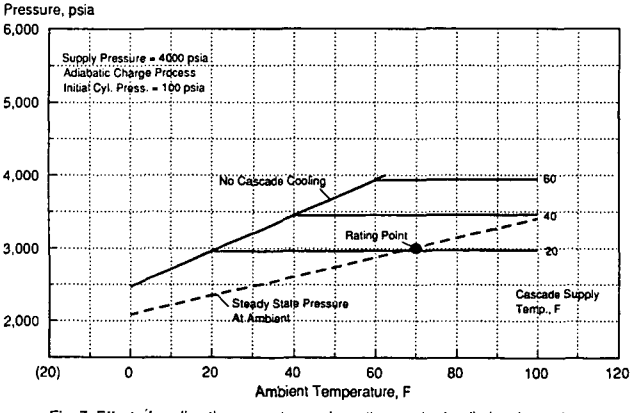

Fig. 7 Effect of cooling the cascade supply on the required cylinder charged pressure

AN INVESTIGATION OF THE USE OF ODORANTS IN LIQUEFIED NATURAL GAS USED AS A VEHICLE FUEL

Thomas Green, Ted Williams
Gas Research Institute, Chicago, Illinois 60631
Richard Bukacek, Prasan Chowdiah
Institute of Gas Technology, Chicago, Illinois 60632

Key Words: Liquefied Natural Gas, LNG Odorization, LNG Vehicles

ABSTRACT

Interest in liquefied natural gas (LNG) as an alternative vehicle fuel has increased significantly. Its greater storage density relative to compressed natural gas makes it an attractive option for both volume and weight constrained vehicle applications. The public transportation market, specifically transit bus properties, have been very aggressive in pursuing LNG as an alternative vehicle fuel. Naturally, when dealing with the general public and a new transportation fuel, the issue of safety must be addressed. With this in mind, the Gas Research Institute has initiated a number of safety related studies including an investigation of the use of odorants in LNG. This paper presents the preliminary results of an investigation performed by the Institute of Gas Technology to determine both the applicability and effectiveness of odorizing LNG. This includes an overview of the current state-of-the-art in LNG vehicle fueling and safety systems as well as a discussion of an LNG odorization program conducted by San Diego Gas & Electric in the mid 70s'. Finally, the paper discusses the results of the modeling effort to determine whether conventional odorants used in natural gas can be injected and remain soluble in LNG at temperatures and pressures encountered in LNG fueling and on-board storage systems.

INTRODUCTION

Interest in LNG vehicles and LNG refueling systems is growing due to the clean burning characteristics of natural gas and the abundant supply of natural gas in North America. As directed by many U. S. codes, natural gas distributed to customers is odorized to the extent that its presence in the atmosphere is readily detectable at gas concentrations of one-fifth of the lower explosive limit. Although LNG is currently not odorized, odorization may provide a significant increase in safety for over the road transportation of LNG and LNG vehicles. Unfortunately, the cryogenic temperature (-260°F) of LNG results in the immediate solidification of any known odorant. Therefore, special odorants and blending techniques must be developed to provide for the proper and effective odorization of LNG.

The objective of this paper is to present potential odorants (or odorant mixtures) and carriers for service in LNG. This includes an evaluation of the concentration of candidate odorants necessary to achieve an acceptable warning level and also the concentration level at which the candidate odorant reaches the solubility limit in LNG and the potential carrier.

SAFETY SPECIFICATIONS

In the United States, detection by odor is typically required before concentrations of natural gas in air reach 1/5th the lower combustible limit of the gas. That is, before natural gas concentration in air reaches 1%. It is implied that a large fraction of the adult population shall recognize the odor when the natural gas is diluted 100 to 1 in air.

Although human response to odors has long been studied, there has been to date little agreement on the theoretical basis for selecting odorants. A widely accepted measure of odorant effectiveness is the "median threshold" level: that concentration in air at which 50% of a test group can consistently detect the presence of the odor without necessarily being able to identify it. "Recognition" level, where 50% of a test group can characterize the odor, is said to be 2 to 5 times the threshold, Kniebes[3], but it is not often reported as measured.

More recently, Ripley et al.[6], introduced the concept of "Warning Level" at which an extrapolation of threshold data to 100% of a population experiencing threshold is the warning level. This definition of warning concentration has its foundation in theory and experiment, and it yields results that compare well with field practice and the data of Ripley. The factor 5 means that most of the population experiences this concentration as very much larger than 5 times their threshold. For t-butyl mercaptan, for example, 50% of the population should experience this odor at a concentration more than 120 times their threshold experience; for thiophane 44 times threshold. Note that the factor 5 is reasonable for odorizing LNG but not where odor fading is likely, i.e., odorizing gas for a transmission or distribution system.

SOLUBILITY

The presence of solids in the flow lines and fittings from an LNG storage tank to an engine can reduce or stop the flow of fuel. Thus, for potential odorants in LNG, it is important to know their solubility limits in LNG, that is, the concentration at which solid odorant begins to precipitate out of solution. A second solubility issue arises in consideration of procedures for introducing odorant into LNG. Because the triple point of candidate odorants are all above the temperatures at which LNG will be stored, the pure

odorants cannot be cooled to LNG temperature prior to placement in LNG. It is useful to consider dissolving the odorant into a carrier liquid and subsequently cooling the carrier/odorant mixture to LNG temperature. The candidate carrier liquids include only Propane and i-Butane.

It is always preferable to have experimental solubility data. In the event such data cannot be found then solubility can be estimated on the following thermodynamic basis. The solid at the triple point of pure material is used as a reference point. The solid is cooled to temperature at which the solubility limit is desired and its fugacity is calculated along this path. The pure liquid is cooled from the triple point to the temperature of interest, then mixed with the LNG: the fugacity of the odorant in solution is calculated along this path. At equilibrium the two fugacities thus calculated must be equal and the limiting concentration in the liquid phase can then be computed.

H = enthalpy
F = Gibbs free energy
S = entropy
f = fugacity
Hfusion = heat of fusion
T = absolute temperature
v = volume
Cp = specific heat
a = activity coefficient

subscripts
o - reference state
s - solid
l - liquid
i - component i
t - temperature
p - pressure

$$F = H - TS, \qquad (dF/dT)p = -S, \qquad (dF/dP)t = v;$$

For the solid at T

$$S_S = S_O + \int C_{ps}\, dT / T$$
$$F_i = F_S = F_O - \int (S_O + \int C_{ps}\, dT / T)\, dT$$

For the liquid at T

$$S_l = H_{fusion} / T_t + \int C_{ps}\, dT / T$$
$$F_l = F_O - \int (S_O + H_{fusion} / T_t + \int C_{ps}\, dT / T)\, dT$$

For the odorant in solution at T

$$F_i = RT\ln(a_i x_i) + F_l = F_S$$

The activity coefficient can be estimated from Scatchard's equation[2] as discussed by Preston and Prausnitz[5].

$$\ln(a_i) = v_i V_j ((d_i - d_j)^2 + 2L_{ij} d_i d_j)/RT$$

Here:

- vi = the molar volume of the odorant at temperature T
- Vfj = the volume fraction of the solvent
- di and dj = the solubility parameters of odorant and solvent
- Lij = a parameter characterizing the interaction of i and j
- R = the gas constant in appropriate units.

The solubility parameters are effectively the internal energy change on vaporizing a unit volume of the liquid at 298.16°K and they characterize the cohesive energy density of a chemical. The activity coefficient calculated by this method is very sensitive to the term Lij: a value of 0 leads to maximum solubility, a value 0.08 to a very low solubility. In the absence of experimental data to guide the selection of Lij, it will be important to choose an extreme value, say 0.08, so that the limiting case solubility has been estimated.

Where the integrations cited above are over a relatively small temperature range and vapor/liquid equilibrium data can be used to calculate values for Lij, then it is not necessary to choose the limiting case value. Such data are available for thiophane, t-butyl mercaptan, isopropyl mercaptan, dimethyl sulfide and ethyl mercaptan in vapor/liquid equilibrium with propane.

There are data available for the solubility of t-butyl mercaptan in methane and LNG[4], but the temperature interval between t-butyl mercaptan's triple point, 274.26°K and LNG temperature, 112°K is such that a useful value of the integrals cited above cannot be adequately evaluated. For its solubility in propane the following limiting case approach was made: For several values of Lij for methane-t butyl mercaptan the integral was evaluated from the product xi*ai at 112°K with xi from Reference 4, then the solubility in propane was evaluated with Lij from vapor-liquid equilibrium data. On inspection of results a conservative value of the integral was selected to enable calculation of t-butyl mercaptan solubility in propane adequate for the screening process of this work.

Fortunately, AIChE's data compilation[1] provides up-to-date correlations for the heats of fusion, densities and specific heats of liquid and solid, and solubility parameters of the chemicals of interest here: various odorants, methane and the potential odorant carriers propane and i-butane. Table 1. lists the solubility limits for promising candidate odorants in methane with Lij = 0.08 (worst case) with their warning concentrations, both in ppm. It is clear that all are adequately soluble in methane and LNG.

TABLE 1. ODORANT SOLUBILITY AND REQUIRED CONCENTRATIONS IN METHANE

Odorant	Solubility, ppm	Warning Concentration, ppm
Ethyl Mercaptan	3785	0.4
i-Propyl Mercaptan	1746	0.6
n-Propyl Mercaptan	630	1.5
i-Butyl Mercaptan	941	1.0
t-Butyl Mercaptan	68	0.1
Thiophane	5	0.6
Dimethyl Sulfide	419	2.9

Values of Lij can be obtained from vapor-liquid equilibrium data. At the low vapor pressures of the odorants it is enough to have values of Ki = yi/xi in a given solvent to get ai = P*Ki/Pi. Here yi and xi are the mole fractions of odorant in the vapor and liquid phases, P is the total pressure and Pi is the vapor pressure of the odorant. The value of Lij thus evaluated at several temperatures should be temperature independent and applicable to estimating the solubilities in the solvent at LNG temperature. The data of Ng and Robinson[7] were used to evaluate Lij for ethyl, isopropyl and t-butyl mercaptans, and dimethyl sulfide dissolved in propane; Whisman et al. data[8] for Lij of thiophane in propane. The values of Lij and the solubilities of these compounds in propane are shown in the Table 2.

TABLE 2. ODORANT SOLUBILITY IN PROPANE

Odorant Name	Lij	Solubility limit ppm in Propane
Ethyl Mercaptan	0.032	83700
Isopropyl Mercaptan	0.042	27600
t-Butyl Mercaptan	0.044	736
Dimethyl Sulfide	0.031	7976
Thiophane	0.029	673

Note that the processes for evaluation require estimation of the properties of the subcooled liquid, but experimental data will be available only for saturated liquid. To test the validity of integration of the correlations of specific heat into the subcooled region an alternative extrapolation procedure was used and the two results compared. The alternative was a linear extrapolation from the triple point with the rate of change of Cp with temperature that at the triple point. Integrations from the triple points to 112° K for 9 potential odorants differed, on absolute average less than 0.2%, with the maximum deviation 0.5%. These results show that the extrapolations are justified, and they lend credence to the programming that implements the process of evaluation. Note also that pressures are low and the molar volume of solids and liquids are small. Thus neglecting the integral (vs-vl)dp will involve negligible error.

It will be observed that the activity coefficient is a function of odorant concentration so that the solubility limit can not be determined in a single step. In this work it was sufficient to start with the concentration estimated for ai=1 to calculate an initial value for solubility: the value for solubility was used to obtain a new value for ai which enabled calculation of a new solubility and the process was repeated until changes in solubility were less than 0.02% of the previous value.

In practice it is desirable to use relatively small amounts of carrier, in the range of 1 gallon carrier to 1000 gallons of LNG. These small amounts will not appreciably affect the composition of the liquid methane
(> 99.5% pure CH_4) being used by an increasing number of fleets. The concentration of odorant in carrier can be calculated

$$Co = Cw*(1+(Dl/Dc)*R)$$

Cw	=	the warning concentration of odorant in LNG at 1/5th LEL
Co	=	concentration of odorant in carrier required to achieve Cw warning concentration in LNG
Dl/Dc	=	the ratio of LNG to carrier densities in moles/volume
R	=	the ratio gallons LNG/gallon odorant

The symbol * in Table 3. indicates that the required concentration is greater than the solubility limit shown. At the level of 1 gallon per 1000 gallons of LNG n-propyl mercaptan is probably satisfactory because Lij is almost certainly smaller than 0.08, but n-butyl mercaptan and thiophane would require

experimental data to justify their use. The average value of Lij for thiophane reported above represents a wider scatter of individual values than the others and is therefore less adequate as a basis for estimating limiting solubility. Given the possibility of overdosing odorant under field conditions, the table above suggests that the ethyl, i-propyl and t-butyl mercaptans are best suited to odorization of LNG at the propane to LNG volume ratio of 1/1000.

Table 3. ODORANT REQUIREMENTS WITH PROPANE AS CARRIER

Odorant	Cw, ppm	R=1000 Co	Solubility limit, ppm	Lij
Ethyl Mercaptan	0.4	941	83700	0.032
i-Propyl Mercaptan	0.6	1294	27500	0.042
n-propyl Mercaptan	1.5	3528*	1766	0.08
i-Butyl Mercaptan	1.0	2234	2697	0.08
n-Butyl Mercaptan	1.0	2234*	185	0.08
t-Butyl Mercaptan	0.1	235	746	0.044
Dimethyl Sulfide	2.9	6821	7976	0.031
Thiophane	0.6	1411*	673	0.029

To produce a carrier with the desired concentration of odorant, we can assume the mixing process to take place at 25°C (77°F).

$$Vo = (Co/1000000)*(Dc/Do)*28316/7.48$$

Vo	=	volume of odorant needed, cc odorant/gallon carrier
Co	=	concentration of odorant desired, ppm
Dc/Do	=	ratio of densities in moles/volume, carrier/odorant at 77°F, 28316/7.48 = cc/gallon

Note that, on substitution from the previous relationship between Co and Cw and taking $1 << (Dl/Do)*R$, we have

$$Vo = Cw*((Dl/Do)*R)*28316/7.48e6$$

We see that Vo is for practical purposes independent of the density of the carrier, and is thus as applicable for carriers other than propane. As shown in Table 4., 10 gallons of propane containing 11 cc of t-butyl mercaptan would odorize an LNG trailer load of 10,000 gallons.

Table 4. CUBIC CENTIMETERS OF ODORANT PER GALLON OF CARRIER; (PROPANE)

Odorant	Vo, cc/gal. R=1000
Ethyl Mercaptan	3.0
i-Propyl Mercaptan	5.2
n-propyl Mercaptan	13.6
i-Butyl Mercaptan	10.3
n-Butyl Mercaptan	10.2
t-Butyl Mercaptan	1.1
Dimethyl Sulfide	21.2
Thiophane	5.3

ODORANT CONCENTRATION IN EQUILIBRIUM LNG VAPOR

It is clear that all the odorant in LNG will be released to the surroundings if the liquid is totally evaporated. But the odorant concentration of the vapor in equilibrium with LNG liquid or of the vapors leaving an LNG spill are not going to be that of the original LNG. To establish the concentration of odorant in the vapor over LNG liquid the following process was used: Taking the reference states of pure component odorant and methane as 112°K and the vapor pressure of the odorant at 112°K, the equality of fugacities in the liquid and vapor phases can be expressed in terms of mole fractions

$$yi = ai*xi*Pi/P$$

Here:

ai	=	the activity coefficient of the odorant
yi, xi	=	the mole fractions of odorant in the vapor and liquid respectively
Pi	=	the vapor pressure of the odorant at T temperature
P	=	the pressure of the equilibrium mixture at T

The activity coefficient can be estimated from Scatchard's equation[2] as discussed by Preston and Prausnitz[5], and described above. The activity coefficient calculated by this method is very sensitive to the term Lij: a value of 0 leads to the minimum values for ai and yi; a value of 0.08 is extreme, and leads to very high values for ai and yi. Use of the value Lij = 0.08 therefore leads to an optimistic value for the concentration of odorant in the vapors in equilibrium with LNG. The values of 0.0 and 0.08 were used to screen potentially useful odorants. If, with Lij = 0.08, the concentration of odorant if far below the threshold level, then certainly the vapor will not be detected by its odor.

Daubert[1] and Danner's data compilation provides data for the vapor pressures, densities and solubility parameters of methane, ethane, propane and i-butane, and a variety of candidate odorants. Because LNG temperature is well below the triple point of the liquid where the pure odorant exits only as a solid, it is necessary to estimate the vapor pressure of the liquid by extrapolation. Two methods suggest themselves: 1) use the correlation of vapor pressure presented by Daubert and Danner at temperatures below the triple point and 2) assume the form ln(Pi) = A/T+B, and calculate the vapor pressure by evaluating dln(Pi)/dT and Pio at the triple point, so that Pi = Pio*exp((T-Tio)*(dln(pi)/dt)). To estimate yi, both values of Pi were calculated and the larger one used in the calculation. Because it is likely that the true values lie between the two, the larger value gives a conservative estimate given that the results are far below the warning level.

With odorant concentration of 5 ppm in methane, Lij = 0.08, T = 112°K, and p=16 psig, values of yi were calculated for 8 odorant candidates with the results shown in Table 6. For all odorants values of yi are far below that needed to obtain threshold concentrations when mixed with air at 1/5th the lower flammable limit for methane.

TABLE 6. ODORANT CONCENTRATION IN METHANE VAPOR

Odorant	yi, ppb	Pi, psia	ai	Ki=yi/xi
Ethyl Mercaptan	0.000200	3.9e-9	166	4e-8
i-Propyl Mercaptan	0.000043	8.6e-10	158	8.6e-9
n-Propyl Mercaptan	0.000129	8.9e-10	459	2.6e-8
n-Butyl Mercaptan	0.000004	1.0e-11	1203	8.0e-10
i-Butyl Mercaptan	0.000000	1.5e-12	598	-
t-Butyl Mercaptan	8.5	2.6e-4	103	1.7e-3
Dimethyl Sulfide	0.0234	4.0e-7	187	4.7e-6
Thiophane	0.000139	2.2e-11	20000	2.8e-8

All are far below the parts per million levels required for detection by odor. T-butyl mercaptan seems an anomaly in this list, but that is probably because the extrapolation from the triple point, 264.26°K, down to 112°K is so far that the estimate of Pi is much lower than the true value.

Vapor in equilibrium with LNG that is released into the atmosphere will not be detected by its odor: the concentration of odorant is just too small. However, the issue is not closed because the plausible occurrences and magnitude of such releases has not yet been established. Furthermore, LNG droplets or aerosols may emanate from the boiling liquid and become entrained in the escaping gas. To the extent that this may occur, additional odorant may be present in the released vapor.

CONCLUSION & RECOMMENDATIONS FOR ODORANTS & CARRIER

The elimination of some candidate carriers is quite easy: n-butane and the heavier hydrocarbons can be immediately eliminated as carriers because their freezing points are too high. Ethane is not a desirable carrier because its critical temperature, 90.1°F, is within the range of ambient temperatures so that phase densities can radically change with small temperature or pressure changes while mixtures are being make or transferred. Only propane and i-butane are sensible candidates, commercially available and typical components of LNG. Propane is clearly preferable to i-Butane because it is more universally available, and its phase equilibrium with odorants has received more experimental attention.

Although 10 mercaptans, hydrogen sulfide, dimethyl sulfide and thiophane were examined during this work, only 3 were found to satisfy the following criteria:

1. There exist adequate experimental data on its odor detection to define the warning concentration of odorant required in LNG. This rules out sec-butyl mercaptan.

2. Concentration of odorant in propane carrier, with Carrier/LNG ratio 1/1000, is well below the solubility limit with the warning concentration delivered to the LNG. Note that the warning concentration for most odorants is well below their solubility in LNG. This rules out thiophane.

3. At the propane/LNG ratio of 1/1000, any plausible overdose of odorant during mixing of odorant with propane will not lead to formation of solids when the result is cooled to LNG temperatures. This rules out all but the ethyl, i-propyl and t-butyl mercaptans on the basis of the experimental data available at present.

4. The odorant is not identified as acutely toxic by EPA - this rules out methyl mercaptan and dimethyl sulfide.

5. The odor in air is perceived as "gassy". This rules out dimethyl sulfide.

The acceptable candidate odorants are:

Ethyl Mercaptan
i-Propyl Mercaptan
t-Butyl Mercaptan

REFERENCES

1. Daubert, T.E. and Danner, R.P., "Physical and Thermodynamic Properties of Pure Chemicals", Design Institute for Physical Property Data, AIChE, Hemisphere Publishing Corporation, New york, 1991

2. Hildebrand, J.H. and Scott, R.L., "Solubility of Nonelectrolytes", Dover, New York, 1964

3. Kniebes, D.V.,"The nose as a Natural Gas Odorant Detector" p.24, IGT Odorization Symposium , Aug. 1980)

4. Kuebler, G.P. and McKinley, C., "Solubility of Solid tert-Butyl Mercaptan in Liquid Methane and an LNG Mixture", Advances in Cryogenic Engineering, V0l 25, 616-619, Plenum Press, N.Y., 1979

5. Preston, G.T. and Prausnitz, J.M., Thermodynamics of Solid Solubility in Cryogenic Solvents, Ind. Eng. Chem. Process Des. Develop., Vol 9, No 2, 1970

6. Ripley D.L. and Goetzinger, J.W. "LP-Gas Odorants", Proceedings of the IGT Odorization Symposium, Sept 1992

7. Robinson, D.B. and Ng,H.J., "VLE Data and Correlations for Odorants in Propane." Symposium on LP-Gas Odorization Technology Proceedings, Dallas, TX, April 1990

8. Whisman, M.L.; Goetzinger, J.W.; Cotton, F.O.; Brinkman, D.W.; and Thompson, C.J., "A New Look at Odorization Levels for Propane Gas," BERC/RI/77/1, 1977

FUEL COMPOSITION EFFECTS ON NATURAL GAS VEHICLE EMISSIONS

Christopher F. Blazek, John Grimes, and Patricia Freeman
Institute of Gas Technology, Chicago, Illinois 60632
Brent K. Bailey and Christopher Colucci
National Renewable Energy Laboratory

Keywords: Natural Gas Vehicles, Natural Gas Composition, NGV Emissions

ABSTRACT

Under a contract from DOE's National Renewable Energy Laboratory (NREL) and support from Brooklyn Union Gas Company (BUG), Northern Illinois Gas Co., the Institute of Gas Technology (IGT) evaluated four state-of-the-art, electronic, closed-loop natural gas vehicle (NGV) conversion systems. The systems included an Impco electronic closed-loop system, Mogas electronic closed-loop system, Stewart & Stevenson's GFI system, and an Automotive Natural Gas Inc. (ANGI) Level I electronic closed-loop conversion system. Conversion system evaluation included emission testing per 40 CFR Part 86, and driveability. All testing was performed with a 1993 Chevy Lumina equipped with a 3.1 L MPFI V6 engine. Each system was emission tested using three different certified compositions of natural gas, representing the 10th, mean and 90th percentile gas compositions distributed in the United States. Emission testing on indolene was performed prior to conversion kit testing to establish a base emission value. Indolene testing was also performed at the end of the project when the vehicle was converted to its OEM configuration to ensure that the vehicle's emissions were not altered during testing. The results of these tests will be presented.

INTRODUCTION

A number of conversion systems are commercially available to convert gasoline fueled vehicles to either dedicated or bi-fueled natural gas vehicles (NGVs). This paper presents the research results to date of four NGV conversion systems tested on the 1993 3.1L MPFI Chevrolet Lumina passenger car. This study included fuel emission testing based on the Federal Test Procedure (FTP) per 40 CFR Part 86 and fuel economy measurements using three different compositions of natural gas. Emission testing on indolene was performed prior to conversion system testing to establish gasoline base emission values. Any variations in emissions or fuel economy related to fuel quality will be better understood as a result of the FTP emission testing program. In addition to fuel quality, this investigation also evaluated conversion system performance, both in terms installation and driveability. All procedures required to convert the gasoline fueled vehicle to compressed natural gas (CNG) were fully documented including hardware installation, electronic hookups, and system calibration.

SPECIFICATION OF NATURAL GAS COMPOSITION

Natural gas is not pure methane or a homogeneous mixture, but varies in composition by location and seasonally. Variations occur between the originating fields and may be further modified due to processing prior to transmission. Additional mixing of different gases also occurs during pipeline transmission. As a result, natural gas does not describe a single type of fuel or a narrow range of characteristics, unlike gasoline or diesel fuel which is manufactured within certain specifications.

Fuel composition can affect vehicle emissions. The most recent work on natural gas composition was completed in 1991 by the American Gas Association Laboratories with the Institute of Gas Technology as a subcontractor, under Gas Research Institute funding.[1] The research focused on the mean average, minimum, maximum, 10th percentile, and 90th percentile gas fractions. However, information reported in the GRI sponsored study for the mean, 10th percentile, and 90th percentile values for each of the component gases allowed for only a pseudo-composition to be developed. For example, the 10 percentile value of methane could be combined with the 90th percentile values of the other constituents for a minimum-methane concentration natural gas. The rationale for this approach is that, when methane dominates the composition, the other gases would be expected to be at their lower values. However, this does not take into account that natural gas compositions are not manufactured but occur normally with certain relationships between each of the components. As a result, IGT concluded that a more detailed review was necessary to determine representative natural gas compositions.

Two primary factors that impact emissions and directly describe the general characteristics of natural gas include the concentration of methane and the Wobbe number. The methane concentration is a good measure because it is the dominant component in natural gas. The Wobbe number is a measure of the fuel energy flow rate through a fixed orifice under given inlet conditions. It is calculated as the ratio of the higher heating value divided by the square root of the specific gravity. Variations in Wobbe number of the gas will produce similar variations in the air-fuel ratio for gas metering systems used on vehicles. Variability of this parameter will most significantly affect engines equipped with open-loop controls, where the exhaust oxygen cannot be sensed and adjusted. In general, the Wobbe number is a good criteria for natural gas because it correlates well with the ability of an internal combustion engine to use a particular gas. It also takes into account many of the gas components because it is a bulk property.

The first step was to determine the minimum, maximum, mean average, median, 10th percentile, and 90th percentile values for the methane mole fraction, as shown in Table 1. This data represents over

6,000 gas samples taken from various locations throughout the continental U.S. It should be noted that the minimum value represents propane/air peakshaving gas. This gas is generated by many local utilities during severe periods of high demand which typically occur during the coldest periods of the year. During mild winters these plants may not even be used and during normal winters plants may only operate 1 to 2 days per year. The equivalent values for the Wobbe number are shown in Table 2.

TABLE 1. METHANE FRACTION ANALYSIS

Minimum:	55.8%
Maximum:	98.1%
Mean (avg):	93.0%
Std Deviation:	4.5%
Median:	94.9%
10th Percentile:	84.1%
90th Percentile:	96.3%

TABLE 2. WOBBE NUMBER ANALYSIS

Minimum:	1202.6
Maximum:	1418.7
Mean (avg):	1329.4
Std Deviation:	42.6
Median: 1347.0	
10th Percentile:	1233.0
90th Percentile:	1358.5

Having identified the methane fraction and Wobbe number values to be used, the next step was to define a suitable method of calculating the mole fractions of each of the other components. Because of the inherent variability of an individual natural gas sample, it was unlikely that a representative composition could be formulated from just the few values that fit exactly on the selected Wobbe number values. To select a slightly wider, more representative range of natural gas compositions at a given value, the average of each of the components was calculated considering only those samples within 2 Wobbe number counts of the identified Wobbe number. These results are shown in Table 3 (values presented are mole %). The near equivalency between methane fraction and Wobbe number for the natural gas composition can be seen in comparing the resulting averages for each of the components in each of the desired ranges. For example, the methane and Wobbe number for the two 10th percentile compositions are fairly close, 83.84 mole % vs. 83.96 mole % and 1229.76 vs. 1232.97. This holds true for the other components. Although there is more variability within the mean and 90th percentile compositions, the differences are within the variations that may be seen throughout the year.

TABLE 3. COMPOSITION BASED ON WOBBE NUMBER

	10%-ile	Mean	90%-ile
METHANE	83.96	92.87	94.80
ETHANE	5.72	3.34	3.03
PROPANE	1.07	0.63	0.58
I-BUTANE	0.09	0.07	0.10
N-BUTANE	0.11	0.12	0.13
I-PENTANE	0.03	0.04	0.05
N-PENTANE	0.01	0.03	0.03
C6+	0.03	0.05	0.07
NITROGEN	6.05	2.07	0.56
CO_2	1.40	0.78	0.65
O_2	1.53	0.00	0.00
WOBBE	1232.97	1329.15	1358.61

Because fuel metering is a critical factor in all NGV conversion systems, both IGT and NREL agreed that the gas compositions based on the Wobbe number, as presented in Table 3, should be used for the test fuels. High pressure gas cylinders were then prepared for each of the three compositions and certified by IGT for use in this test program.

BASELINE EMISSION TEST

IGT leased a new 1993 Chevy Lumina 3.1 liter MPFI V6 (VIN# 2G1WN54T7P9146384) for the testing program. During December of 1992 and January of 1993 the vehicle was driven 5,000 mostly highway miles on gasoline to ensure proper engine break-in and catalyst aging. An inspection was performed on the Lumina at 4,803 to establish baseline parameters prior to emission testing and conversion.

FTP emission testing on indolene were initiated in March, 1993 per 40 CFR Part 86 on the Chevy Lumina. Two baseline indolene tests were performed with the dynamometer set for a 3,500 pound inertia and 6.0 ahp. The vehicle odometer read 6,410 miles. The test results are presented in Table 4. As can be seen from the test results, the vehicle passed the exhaust emissions and shed test. Weighted total hydrocarbon values were 0.23 and 0.27, carbon monoxide 2.74 and 2.84, nitrous oxides 0.48 and 0.49, carbon dioxide 489 and 491, respectively reported in grams per mile, with fuel economy for both tests at 18.0 mpg. The shed test results were 0.34 and 0.39 grams respectively.

CNG EMISSION TEST RESULTS

All systems were installed and setup according to the manufacturer's instruction. Following the installation, a test drive and dynamometer set-up were performed using a snap-on analyzer for ECM parameters. Power valve and idle adjustment were performed to minimize tailpipe emissions (through the converter) without sacrificing driveability. Following these adjustments, IGT conducted driveability tests following the CRC Report No. 577 "1990 CRC Driveability Workshop" recommendations

published in October 1990.[2] All four systems passed the driveability tests with no faults and did not experience engine stalling or hesitation, nor any problems with starting.

TABLE 4. EXHAUST AND EVAPORATIVE INDOLENE EMISSIONS DATA

Test Fuel	Indolene		
Test Date		3/12/93	3/15/93
Vehicle Odometer, miles		6410	6429
Exhaust Emission Results			
Cold Transient, grams			
	THC (C_3H_8 calibration)	2.65	3.15
	CH_4 (a)	0.22	0.26
	NMHC (a)	2.40	2.85
	CO	23.24	26.97
	NO_x	4.25	3.95
	CO_2	1741	1767
	Fuel Economy, MPG	17.9	17.6
Cold Stabilized, grams			
	THC (C_3H_8 calibration)	0.34	0.25
	CH_4 (a)	0.12	0.12
	NMHC (a)	0.20	0.11
	CO	4.70	4.32
	NO_x	1.14	1.21
	CO_2	1992	2004
	Fuel Economy, MPG	17.9	17.0
Hot Transient, grams			
	THC (C_3H_8 calibration)	0.45	0.74
	CH_4 (a)	0.13	0.14
	NMHC (a)	0.29	0.57
	CO	9.82	8.99
	NO_x	1.02	1.22
	CO_2	1533	1536
	Fuel Economy, MPG	20.5	20.5
Weighted Total, grams / mile			
	THC (C_3H_8 calibration)	0.23	0.27
	CH_4 (a)	0.04	0.04
	NMHC (a)	0.19	0.22
	CO	2.74	2.84
	NO_x	0.48	0.49
	CO_2	489	491
	Fuel Economy, MPG	18.0	18.0
Shed, grams			
Diurnal 0.12		0.20	
Hot Soak		0.22	0.19
Total 0.34		0.39	

All emission tests were performed at the AutoResearch Laboratories per 40 CFR Part 86. The dynamometer was set for a 3,500 pound inertia and 6.0 ahp. The preliminary test results for the MOGAS system as tested in April, 1993 are presented in Table 5 for the three different gas compositions. From the weighted total results, it became clear that the vehicle was set-up lean following Mogas's set-up instructions. IGT did not attempt to optimize the emission results during set-up. However, the results do indicate that NO_x emissions could be reduced running richer, and thereby increasing carbon monoxide emissions which are currently significantly below the limit. It should be noted that for the 10th percentile gas the system did not pass the 1993 EPA NOx limit of 1.0 gr./mile.

The preliminary test results for the Impco system as tested in May, 1993 are presented in Table 6. As was the case with the MOGAS system, the weighted total test results indicate that the vehicle was set-up lean following Impco's set-up instructions. IGT did not attempt to optimize the emission results during set-up. Again, the results indicate that NO_x emissions could be reduced running richer, and thereby increasing carbon monoxide emissions which are currently significantly below the limit. However, the system met all applicable 1993 EPA emission standards for the entire range of natural gas compositions tested.

The preliminary test results for the GFI system as tested in July, 1993 are presented in Table 7. From weighted total results for the mean gas composition, it became clear that the vehicle was set-up rich by the GFI provided software. The carbon monoxide average (4.04 g/mile) was above the 3.4 g./mile EPA limit. However, the results do indicate that CO emissions could be reduced running leaner, and thereby increasing NOx emissions which are currently significantly below the limit. Since the software version supplied by GFI is specific to the 1993 Lumina tested, software changes may be required to "re-calibrate" the vehicle.

The weighted total results for the 90th and 10th percentile gas compositions further confirmed that the vehicle was set-up rich by the GFI provided set-up software. However, a closer analysis of the test results by IGT indicated that the 90th and the 10th percentile gas composition tests did not concur with

the repeatability guidelines set forth in the publication "Statistical Design and Analysis Methods for the Auto/Oil Air Quality Research Program" as published by Painter and Rutherford in SAE paper 920319.[3] Of the tests reported, the HC, CO, and NO_X cold stabilized test pairs and the HC weighted total values from the 90th percentile gas composition did not meet this criteria. Likewise for the tests conducted on 10th percentile gas composition, the NO_X and HC cold transient test pairs and the HC, CO, and NO_X hot transient pairs also were above the limiting ratios. Further investigation indicated that an "air leak" in the testing equipment may have been a contributing cause to these differences.

As a result of this discrepancy noted above, a third test was performed for just the 90th and 10th percentile gas compositions to verify that the "air leak" was corrected and to provide further correlation of the test results. The data for these additional tests are summarized in Table 7 along with the previous test data. As can be seen, the 90th and 10th percentile "third" test data agree more closely to the "first" tests performed on each composition. However, based on the Auto/Oil reference sited above, IGT took the recommended approach of averaging the three tests for the average values reported for the 90th and 10th percentile gas composition tests.

Based on the average values for each of the gas compositions, the GFI system failed the CO emissions test based on the 1993 CO standard of 3.4 g/mi. However, two factors must be taken into consideration when assessing the GFI system. Both the related NOx emission values and the system setup requirements and system sophistication. Unlike the previous two systems tested, the GFI system requires information about the gas composition during vehicle setup and calibration. For this test IGT used the system default values and did not attempt to "dial in" the gas composition for each of the three gas compositions tested. Since the other two systems were not "tuned" on each composition, it was decided that this would give the GFI system an advantage. Second, and even more important, unlike the other systems, the GFI system incorporates a built in learning algorithm in the electronic controls which gradually adjusts the fuel/gas mixture in response to operating parameters such as exhaust oxygen sensor output relative to load. This learning adjustment occurs gradually during normal driving. However, due to the nature of the emission testing, the vehicle was not driven between tests to allow the system to adjust to the new fuel composition. Because of the cost of the certified test fuel, driving between tests was not deemed practical. Since the GFI system incorporates an adaptive learning electronic control system, given enough time on a given gas composition, this system may have passed all of the emission standards. The very low and consistent NOx levels of the GFI system also suggest that this system may have the capability of meeting 1994 standards, even on the 1993 test vehicle

The preliminary test results for the ANGI system as tested in October, 1993 are presented in Table 8. From weighted total results for the mean gas composition, the average levels of CO and NO_X emissions are well below the current EPA limits. The weighted totals for the 10th percentile composition indicate that the ANGI system failed the current NO_X standard of 1.0 g/mile. This indicates that the system produced very low emission levels with the mean composition gas, but the 10th percentile composition caused the system to run too lean.

The test results for the 90th percentile gas composition for the levels of CO did not concur with the repeatability guidelines set forth in the Auto/Oil reference. Again, based on Auto/Oil recommendations, a third test was performed. The results of the second and third tests were within recommended limits. Since there was a possibility of high background levels of CO during the first test and since the second and third test results were in close agreement, the first test was treated as an outlier and the average results were taken from tests 2 and 3. Thus, the weighted total test results for the 90th percentile were well within the EPA limits for CO and NO_X. This indicates that the ANGI system operates well on the mean and 90th percentile compositions which have a higher methane content, but the system fails current EPA limits on NO_X emission levels when operating with 10th percentile gas composition fuel.

CONCLUSIONS

As can be seen from these results, the Mogas system produced the lowest carbon monoxide test results followed by the Impco, ANGI and GFI systems. The GFI system actually failed the CO emissions test based on the 1993 CO standard of 3.4 g/mi. However, two factors must be taken into consideration when assessing the GFI system. Unlike the other 2 systems, the GFI system requires information about the gas composition during vehicle setup and calibration. For this test IGT used the system default values and did not attempt to "dial in" the gas composition for each of the three gas compositions tested. Since the other two systems were not "tuned" on each composition, it was decided that this would give the GFI system an advantage. Second, and even more important, unlike the other systems, the GFI system incorporates a built in learning algorithm in the electronic controls which gradually adjusts the fuel/gas mixture in response to operating parameters such as exhaust oxygen sensor output relative to load. This learning adjustment occurs gradually during normal driving. However, due to the nature of the emission testing, the vehicle was not driven between tests to allow the system to adjust to the new fuel composition. Because of the cost of the certified test fuel, driving between tests was not deemed practical.

TABLE 5. MOGAS SYSTEM EMISSIONS SUMMARY

Fuel Type Mean CNG		
Vehicle Odometer, miles	6821	6832
Exhaust Emission Results		
Weighted Total, grams / mile		
THC (CH_4 calibration)	1.41	1.40
CH_4 (a)	1.40	1.42
NMHC (a)	0.16	0.11
CO	0.39	0.19
NO_x	0.85	0.90
CO_2	363	357
Fuel Economy, MPG	18.9	19.1
Fuel Type 90th Percentile CNG		
Vehicle Odometer, miles	6858	6869
Exhaust Emission Results		
Weighted Total, grams / mile		
THC (CH_4 calibration)	1.28	1.37
CH_4 (a)	1.22	1.34
NMHC (a)	0.16	0.09
CO	0.59	0.28
NO_x	0.79	0.83
CO_2	351	355
Fuel Economy, MPG	19.2	19.0
Fuel Type 10th Percentile CNG		
Vehicle Odometer, miles	6898	6910
Exhaust Emission Results		
Weighted Total, grams / mile		
THC (CH_4 calibration)	1.72	1.98
CH_4 (a)	1.66	2.00
NMHC (a)	0.17	0.18
CO	0.12	0.13
NO_x	1.03	1.01
CO_2	355	359
Fuel Economy, MPG	20.7	20.4

TABLE 6. IMPCO SYSTEM EMISSIONS SUMMARY

Mean CNG		
Vehicle Odometer, miles	7309	7320
Exhaust Emission Results		
Weighted Total, grams / mile		
THC (CH_4 calibration)	1.01	1.03
CH_4 (a)	1.11	1.01
NMHC (a)	0.04	0.05
CO	0.80	0.54
NO_x	0.82	0.83
CO_2	379	376
Fuel Economy, MPG	18.1	18.2
Fuel Type 90th Percentile CNG		
Vehicle Odometer, miles	7280	7291
Exhaust Emission Results		
Weighted Total, grams / mile		
THC (CH_4 calibration)	1.04	0.97
CH_4 (a)	1.03	1.10
NMHC (a)	0.05	0.04
CO	1.74	1.31
NO_x	0.57	0.63
CO_2	378	373
Fuel Economy, MPG	17.8	18.0
Fuel Type 10th Percentile CNG		
Vehicle Odometer, miles	7251	7262
Exhaust Emission Results		
Weighted Total, grams / mile		
THC (CH_4 calibration)	1.65	1.79
CH_4 (a)	1.63	1.82
NMHC (a)	0.14	0.14
CO	0.02	

TABLE 7. GFI SYSTEM EMISSIONS SUMMARY

Fuel Type	Mean CNG		
Vehicle Odometer, miles	7620	7630	
Exhaust Emission Results			
Weighted Total, grams / mile			
THC (CH_4 calibration)	1.31	1.21	
CH_4 (a)	1.30	1.26	
NMHC (a)	0.08	0.07	
CO	4.16	3.92	
NO_x	0.18	0.22	
CO_2	389	394	
Fuel Economy, MPG	17.3	17.1	
Fuel Type	90th Percentile CNG		
Vehicle Odometer, miles	7650	7661	7854
Exhaust Emission Results			
Weighted Total, gr. / mile			
THC (CH_4 calibration)	1.27	0.77	1.18
CH_4 (a)	1.20	0.79	1.36
NMHC (a)	0.07	0.05	0.05
CO	4.27	2.56	4.05
NO_x	0.22	0.19	0.27
CO_2	373	378	382
Fuel Economy, MPG	17.8	17.7	17.4
Fuel Type	10th Percentile CNG		
Vehicle Odometer, miles	7691	7710	7873
Exhaust Emission Results			
Weighted Total, gr. / mile			
THC (CH_4 calibration)	1.05	1.04	1.00
CH_4 (a)	1.07	1.01	1.02
NMHC (a)	0.08	0.07	0.07
CO	3.40	3.16	3.36
NO_x	0.23	0.19	0.26
CO_2	395	377	386
Fuel Economy, MPG	18.5	19.4	18.9

TABLE 8. ANGI SYSTEM EMISSIONS SUMMARY

Fuel Type	Mean CNG		
Vehicle Odometer, miles	8610	8621	
Exhaust Emission Results			
Weighted Total, grams / mile			
THC (CH_4 calibration)	0.52	0.50	
CH_4 (a)	0.49	0.52	
NMHC (a)	0.04	0.03	
CO	1.40	1.29	
NO_x	0.11	0.12	
CO_2	384	385	
Fuel Economy, MPG	17.9	17.8	
Fuel Type	90th Percentile CNG		
Vehicle Odometer, miles	8670	8681	8808
Exhaust Emission Results			
Weighted Total, g / mile			
THC (CH_4 calibration)	0.78	0.54	0.56
CH_4 (a)	0.82	0.53	0.58
NMHC (a)	0.04	0.03	0.05
CO	5.05	1.95	1.60
NO_x	0.09	0.18	0.10
CO_2	397	392	394
Fuel Economy, MPG	16.7	17.2	17.1
Fuel Type	10th Percentile CNG		
Vehicle Odometer, miles	8632	8651	
Exhaust Emission Results			
Weighted Total, g / mile			
THC (CH_4 calibration)	0.92	0.92	
CH_4 (a)	0.94	1.06	
NMHC (a)	0.06	0.06	
CO	0.23	0.24	
NO_x	1.09	1.46	
CO_2	387	428	
Fuel Economy, MPG	19.1	17.2	

(a) CNG Tests: Methane concentration is based on independent GC analysis. NMHC calculation from GC speciation analysis.

With respect to the average NOx emission level , the GFI system produced the lowest NOx test results for all compositions followed by the Impco and Mogas systems. The ANGI system produced even lower levels of NOx emissions with the mean and 90th percentile gas compositions, but did not pass the 1993 NOx standard of 1.0 g/mi with the 10th percentile gas composition fuel. The Impco and GFI systems passed the NOx standard while the Mogas system was slightly over the limit. In assessing these results one must take into consideration the system setup procedure. Both the Impco, and Mogas systems involved subjective tuning of the system to achieve low tailpipe emissions based on the use of a 4 gas analyzer. The subjective nature of the setup as well as the system sensitivity resulted in a lean mixture for all three of these conversion systems. This produced a combination of relatively low CO and high NOx, as would be expected. On the other hand, the GFI and ANGI systems calibrate themselves automatically, producing the opposite effect. This automatic rich setup produced surprisingly consistent low NOx values for each of the gas compositions tested, resulting in NOx emissions below both the 1993 and 1994 emission limits, except where noted above.

ACKNOWLEDGMENT

IGT would like to thank Mr. Brent Bailey and Mr. Chris Colucci at the U.S. Department of Energy, National Renewable Energy Laboratory for both their patience and support during this program. Special thanks goes to Ms. Heide Swanson and Mr. Wilson Tomala at Brooklyn Union Gas for supporting the testing of a fourth conversion system. Other organizations that contributed to the success of this program include the Northern Illinois Gas Company, Amoco, the Gas Research Institute and AutoResearch Laboratory as well as the cooperation of the equipment suppliers.

REFERENCES

1. W.L. Liss, W.H. Thrasher, G.F. Steinmetz, P. Chowdiah, and A. Attari, "Variability of Natural Gas Composition in Select Metropolitan Areas of the United States" Gas Research Institute Report No. GRI-92/0123; March 1992.

2. "1990 CRC Driveability Workshop", CRC Report No. 577 October, 1990.

3. Painter, Rutherford, "Statistical Design and Analysis Methods for the Auto/Oil Air Quality Research Program", SAE paper 920319.